Arfgef1 haploinsufficiency in mice alters neuronal endosome composition and decreases membrane surface postsynaptic $GABA_A$ receptors

JiaJie Teoh[1], Narayan Subramanian[1,8], Maria Elena Pero[3,7], Francesca Bartolini[3], Ariadna Amador[1], Ayla Kanber[1], Damian Williams[1], Sabrina Petri[1], Mu Yang[1], Andrew S. Allen[5], Jules Beal[6], Sheryl R. Haut[6], Wayne N. Frankel[1,2]

[1]Institute for Genomic Medicine, [2]Department of Genetic and Development, [3]Department of Pathology & Cell Biology, [4]Irving Cancer Research Center, Columbia University Irving Medical Center, New York, NY.

[5]Department of Biostatistics and Bioinformatics, Duke University, Durham, NC.

[6] The Saul R. Korey Department of Neurology, Montefiore Medical Center and Albert Einstein College of Medicine, Bronx, NY.

[7]Department of Veterinary Medicine and Animal Production, University of Naples Federico II, Naples, Italy.

[8](current address) Department of Electrical and Computer Engineering, University of Florida, Gainesville, FL.

Conflict of Interest

WNF consults for Praxis Precision Medicines, Inc.. JB consults for Upsher-Smith and GW Pharmaceuticals.

Acknowledgements

This research is supported by NIH grant R37 NS031348 to WNF, NIH grant U01HG0009610 to JB and NIH/NIA grant RO1AG050658 to FB. We are grateful to Erin Heinzen-Cox, David Goldstein, Daniel Lowenstein and the EPGP and Epi4k project teams for bringing the *ARFGEF1* variant to our attention, to Osasumwen Virginia Aimiuwu for support in RNA reverse transcription and to Ryan Dhindsa for his R script for determining permutation statistics.

Abstract

ARFGEF1 encodes a guanine exchange factor involved in intracellular vesicle trafficking, and is a candidate gene for childhood genetic epilepsies. To model *ARFGEF1* haploinsufficiency observed in a recent Lennox Gastaut Syndrome patient, we studied a frameshift mutation (*Arfgef1*^{fs}) in mice. *Arfgef1*$^{fs/+}$ pups exhibit signs of developmental delay, and *Arfgef1*$^{fs/+}$ adults have a significantly decreased threshold to induced seizures but do not experience spontaneous seizures. Histologically, the *Arfgef1*$^{fs/+}$ brain exhibits a disruption in the apical lining of the dentate gyrus and altered spine morphology of deep layer neurons. In primary hippocampal neuron culture, dendritic surface and synaptic but not total $GABA_A$ receptors ($GABA_AR$) are reduced in *Arfgef1*$^{fs/+}$ neurons with an accompanying decrease in $GABA_AR$-containing recycling endosomes in cell body. *Arfgef1*$^{fs/+}$ neurons also display differences in the relative ratio of $Arf6^+$:$Rab11^+$:$TrfR^+$ recycling endosomes. Although the $GABA_AR$-containing early endosomes in *Arfgef1*$^{fs/+}$ neurons are comparable to wildtype, *Arfgef1*$^{fs/+}$ neurons show an increase in $GABA_AR$-containing lysosomes in dendrite and cell body. Together, the altered endosome composition and decreased neuronal surface $GABA_AR$ results suggests a mechanism whereby impaired neuronal inhibition leads to seizure susceptibility.

Highlights

1. *Arfgef1*$^{fs/+}$ mice have lower seizure threshold but no spontaneous seizure.
2. *Arfgef1*$^{fs/+}$ neurons show reduced dendritic surface $GABA_AR$.
3. *Arfgef1*$^{fs/+}$ neurons have decreased $GABA_AR$-containing recycling endosome accompanied with an increase in $GABA_AR$-containing lysosomes.

Keywords

Lennox-Gastaut Syndrome, Epilepsy, $GABA_A$ receptor, endocytic cycle.

Introduction

Epileptic encephalopathy (EE) is a group of brain disorders often with childhood onset and accompanied by serious neurocognitive consequences (Jain et al., 2013). While linkage and association studies have suggested that *ARFGEF1* is involved in genetic epilepsy (Wallace et al., 1996; Piro et al., 2011; Addis et al., 2018), it was one of several candidate genes and no specific causal *ARFGEF1* variants were indicted previously.

ARFGEF1 encodes Brefeldin A (BFA) inhibited guanine-nucleotide-exchange protein-1, also known as BIG1 (Addis et al., 2018); and is highly conserved across mammals and eukaryotes (Wright et al., 2014). Arfgef1 belongs to the GBF/BIG family based on the relatively large molecular size compared to other ARF-GEFs and a distinctive feature – sensitivity to Brefeldin A (BFA) (Yamaji et al., 2000). Among multiple domains, the BFA-sensitive Sec7 catalytic domain is the most studied (Le et al., 2013; Lin et al., 2013; Zhou et al., 2013). Arfgef1 selectively activates Class I ARFs to initiate conversion of ARF-GDP to ARF-GTP during the process of intracellular vesicle formation and trafficking (Zhao et al., 2002). Earlier studies

67 also showed that the N-terminal DCB domain interacts with Arl1, targeting Arfgef1 to the
68 trans-Golgi network (TGN) membrane (Galindo et al., 2016); the C-terminus interacts with
69 kinesin and myosin (Saeki et al., 2005; Shen et al., 2008) as well as regulating cell surface
70 localization of ABCA1 or $GABA_AR$ (Lin et al., 2013; Li et al., 2014). The role of Arfgef1 in
71 the TGN has been studied in detail (Manolea et al., 2008; Boal and Stephens, 2010; Lowery et
72 al., 2013), where it activates Arf1-GTP to recruit clathrin coats, AP1 and Arf binding proteins,
73 also known as GGAs (Lowery et al., 2013). These vesicle-forming components with cargo-
74 sorting capability form new vesicles and traffic cargo from TGN to endosomes or plasma
75 membrane (Shen et al., 2006).
76
77 An earlier study suggested that BIG2 (Arfgef2) is functionally associated with endosomal
78 integrity whereas Arfgef1 is associated with the Golgi (Shen et al., 2006). However, newer
79 evidence suggests that Arfgef1 is also localized on endosomes (D'Souza et al., 2014). Since the
80 main Arfgef1 target, Arf1, localizes on recycling endosomes and regulates trafficking from
81 recycling endosome to plasma membrane (Nakai et al., 2013) and GGAs are known to facilitate
82 trafficking between TGN and lysosomes (Hirst et al., 2000), it is reasonable to suggest that
83 Arfgef1 may have a role in post-TGN endosomal trafficking, similar to that of BIG2. However,
84 this aspect of Arfgef1 is understudied.
85
86 Arfgef1 regulates neurite development *in vitro* (Zhou et al., 2013). Recently, different groups
87 demonstrated that Arfgef1 is required both for the survival of cortical deep layer neurons and
88 for the initiation of neuronal myelination (Teoh et al., 2017; Miyamoto et al., 2018). Another
89 *in vitro* study showed that decreased Arfgef1 abundance is coupled with decrease of plasma
90 membrane $GABA_AR$ without affecting total $GABA_AR$, resulting in impaired chloride ion

91 influx (Li et al., 2014). However, it is not yet known directly whether Arfgef1 has a role in
92 phenotypes that rely on maintaining inhibition:excitation balance *in vivo*.
93
94 Understanding the underlying disease etiology and mechanisms may provide insight for new
95 therapies, especially needed for severe childhood epilepsies. Here, we examine the effect of
96 *Arfgef1* haploinsufficiency in a new mouse line based on a Lennox-Gastaut patient that carries
97 a *de novo* loss of function mutation in *ARFGEF1*.
98
99 **Results**
100 ***ARFGEF1 de novo* nonsense mutation in a Lennox-Gastaut Syndrome patient.**
101 *ARFGEF1* was detected as a candidate gene in a boy diagnosed with Lennox-Gastaut
102 Syndrome. Seizures began at 6 months of age, and were subsequently diagnosed as infantile
103 spasms. By 3 years of age, the patient exhibited generalized convulsions as well as myoclonic,
104 tonic, and atonic seizures. Neurological exams showed global developmental delay and axial
105 hypotonia. He had no language and no meaningful vocalizations. He was unable to pull to stand
106 or support his own weight. General physical exam results were normal and no dysmorphic
107 features was observed. The electroencephalogram (EEG) initially showed hypsarrhythmia and
108 infantile spasms. Subsequent EEGs showed the emergence of generalized slow spike-and-wave
109 activity along with paroxysmal fast activity and persistence of multifocal epileptiform
110 discharges, superimposed on a high amplitude, disorganized background. He was treated
111 initially with ACTH, followed by multiple medications including vigabatrin, levetiracetam,
112 clonazepam, zonisamide, phenobarbital, lamotrigine, valproic acid, and rufinamide. He was
113 also treated with the ketogenic diet and underwent a corpus callosotomy. Despite these
114 interventions the seizures remained severely refractory.
115

Exome sequencing performed as part of the Epi4k Collaborative (Epi4K Consortium et al., 2013) revealed a single nucleotide variant resulting in a premature translational stop codon in exon 30 of the *ARFGEF1* gene (ENST00000262215.3:c.4365C>A; p.Cys1455Ter). The patient also has a missense mutation in the *BMP2* gene (ENST00000378827.4:c.328C>A; p.Arg110Ser), classified as "probably damaging" based on a PolyPhen-2 score of 0.968. However, since *BMP2* variants have not yet been associated with neurological disease in human or mouse, and because *Arfgef1* null mouse mutants have abnormal brain development (Teoh et al., 2017), we considered *ARFGEF1* the more likely candidate.

Genetic analysis of *Arfgef1* haploinsufficiency

We generated an *Arfgef1* knockout mouse line on the C57BL/6NJ strain background by using CRISPR/Cas9 to target the orthologous region on mouse Chromosome 1 (Fig. 1A; Methods). Line *Arfgef1*^{em3Frk} (shown hereafter as *Arfgef1*^{fs}) has a 4-nt frameshift mutation in exon 30, resulting in a premature termination codon (MQYVMYSPSI*) closely mimicking the patient's mutation. Although heterozygous mice are viable and fertile, all homozygotes died within one day of birth, similar to a previous report of the *Arfgef1* knockout mouse (Teoh et al., 2017). The presence of cDNA and protein in whole brain at embryonic day 17.5 was examined using primer pairs flanking N-terminal DCB domain, Sec7 domain, exon 29-31 (mutation in exon 30) and C-terminal HDS4 domain (Fig. S1). The Arfgef1 protein was not detected in *Arfgef1*$^{fs/fs}$ whole brain lysate using Arfgef1 antibodies with N-terminal epitopes (Fig. 1B). In *Arfgef1*$^{fs/+}$ brain, Arfgef1 protein was lower in abundance than wildtype, consistent with haploinsufficiency. The brain size of E17.5 embryos from *Arfgef1*$^{fs/+}$ were comparable to wildtype except that the *Arfgef1*$^{fs/fs}$ forebrain was notably smaller.

Developmental delay in *Arfgef1*$^{fs/+}$ mouse pups

We studied the impact of the *Arfgef1*$^{fs/+}$ genotype in mouse pups, to explore parallels with the Lennox-Gastaut Syndrome patient. Newborn pups are known to perform typical behavioral activities that serve as benchmarks for neurodevelopmental delay during postnatal development (Hill et al., 2008). *Arfgef1*$^{fs/+}$ pup body weight did not change significantly from postnatal day (PND) 3 to PND11 (Fig. 2A), suggesting that the feeding behavior was normal. However, in the first week the latency was increased modestly for several tasks, including surface righting reflex and negative geotaxis (Fig. 2B, C), while the vertical screen holding was similar to wildtype (Fig. 2D, E). This is consistant with the hypotonia phenotype found in the patient. Pups younger than PND12 emit ultrasonic vocalization (USV) when separated from dam and littermates (Ferhat et al., 2016). The USV calls in wildtype pups peaked at PND6 and then gradually diminished. In contrast, the peak and diminishment of USV calls was significantly delayed in *Arfgef1*$^{fs/+}$ (Fig. 2F). This indicates developmental delay and is consistent with what was seen in patient. Representative samples of USV calls from wildtype and *Arfgef1*$^{fs/+}$ pups are shown in Fig.S2.

Morphological defects in *Arfgef1*$^{fs/+}$ brains and neurons

An earlier study showed that the *Arfgef1* knockout heterozygotes have normal brain size during embryogenesis (Teoh et al., 2017), but the postnatal brain was not examined. First, we observed that *Arfgef1*$^{fs/+}$ mice showed transient weight loss by PND14, and catch-up to wildtype by PND45 (Fig. 3A). Using this as a guide for histological examination, we then compared *Arfgef1*$^{fs/+}$ and wildtype brain at PND14, PND30 and PND45 (Fig. 3B). The overall brain size of *Arfgef1*$^{fs/+}$ was similar to wildtype, but dysregulated growth in the dentate gyrus lining of *Arfgef1*$^{fs/+}$ hippocampus was apparent from PND30 (Fig. 3B, red arrowheads). We then examined the morphology of single neuron by diolistic labeling using DiI, a lipophilic dye that diffuses through the membrane lipid bilayer and stains the whole cell structure, first in primary

166 neuron culture and then in brain slices. At 14 days *in vitro* (DIV), we observed long,
167 filamentous and tertiary branch-like structures with larger growth cones on the dendrite of
168 *Arfgef1*$^{fs/+}$ primary hippocampal neurons (Fig. 3C, red arrowheads). These tertiary structures
169 did not adhere to the culture dish surface compared to the respective primary dendrite. Larger
170 growth cone size has been shown to correlate with slower neurite growth rate (Ren and Suter,
171 2016), suggesting a delay in dendritic branch maturation. In *Arfgef1*$^{fs/+}$ brain slices, although
172 the total spine density was similar in deep layer neurons of both genotypes (Fig. 3D, 3E), the
173 distribution of spine morphological subtypes was altered. In *Arfgef1*$^{fs/+}$ dendrites, the fraction
174 of mushroom-shaped spines was significantly higher than observed in wildtype (Fig. 3D,
175 bottom inset, red arrowheads), whereas there were fewer thin spines and filopodia (Fig. 3F).
176 Since mushroom spines on cortical deep layer neurons are typically more persistent than the
177 immature thin spines or filopodia (Trachtenberg et al., 2002), this evidence suggested changes
178 in dendritic spine plasticity.
179
180 **Seizure susceptibility of *Arfgef1*$^{fs/+}$ adult mice**
181 In four years of breeding, *Arfgef1*$^{fs/+}$ mice show no signs of spontaneous convulsive seizure
182 throughout their lifetime, nor was there evidence of seizure or epileptiform activity in 48 hr
183 video-EEG recordings of heterozygous adult mice (Fig. S3). However, both male and female
184 heterozygotes have a significantly reduced electroconvulsive threshold to the minimal
185 forebrain clonic seizure endpoint, compared with wildtype littermates (Wilcoxon test with
186 permutation p=0.003 and p=0.001, respectively; Fig. 4A). They are also susceptible to tonic-
187 clonic seizures induced by subcutaneous $GABA_AR$ antagonist pentylenetetrazol (PTZ) at a
188 dose (40 mg/kg) near the threshold for wildtype C57BL/6NJ mice. Thus, 92.7% of *Arfgef1*$^{fs/+}$
189 heterozygotes reached the tonic-clonic seizure or worse endpoint, in contrast to 18.2% of
190 wildtype mice ($p<0.0001$, Fisher's Exact Test). The average latency to the first tonic-clonic

191 seizure was also significantly shorter in *Arfgef1*$^{fs/+}$ mice, by an average of 788 sec (Wilcoxon
192 test with permutation $p<0.001$; Fig. 4B).
193
194 **Decreased dendritic surface GABA$_A$R in *Arfgef1*$^{fs/+}$ neurons**
195 Li and colleagues (2014) previously demonstrated that siRNA-mediated depletion of Arfgef1
196 could reduce functional GABA$_A$R at the membrane surface (Li et al., 2014). Given the
197 morphological features and seizure susceptibility of *Arfgef1*$^{fs/+}$ mice, we examined GABA$_A$R
198 localization in primary hippocampal neuron culture. Through immunofluorescence staining of
199 permeabilized neurons, we determined that the total number of GABA$_A$R puncta in proximal
200 dendrite of *Arfgef1*$^{fs/+}$ was similar to that of wildtype (Fig. 5A, D). However, on non-
201 permeabilized neurons, the dendritic surface bound GABA$_A$R puncta count decreased in
202 *Arfgef1*$^{fs/+}$ (Fig. 5B, E). GABA$_A$R puncta colocalized with synaptophysin, a synaptic marker,
203 also decreased (Fig. 5C, F), together suggesting a decrease in synaptic GABA$_A$R density along
204 the dendritic surface. Initial assessment of synaptic properties of hippocampal pyramidal
205 neurons from these cultures at DIV14 showed that *Arfgef1*$^{fs/+}$ neurons had a nominal increase
206 in mean mEPSC frequency and no difference in mIPSC frequency or in mEPSC or mIPSC
207 amplitude (Figure S4A, B, C).
208
209 **Disrupted distribution of GABA$_A$R-containing trafficking vesicles in *Arfgef1*$^{fs/+}$ neurons**
210 Because the total GABA$_A$R puncta count remained unchanged, we reasoned that the decrease
211 in synaptic GABA$_A$R may result from malfunction either in receptor trafficking or in recycling
212 to the plasma membrane. That is, GABA$_A$R might be endocytosed but cannot be recycled back
213 to plasma membrane (Li et al., 2014), or there is slowdown in trafficking of GABA$_A$R from
214 Golgi to plasma membrane.
215

There is significant heterogeneity in the type and subcellular localization of recycling endosomes in neurons, and this heterogeneity is in part represented by Arf6^{+}, Rab11^{+}, TrfR+ markers. For example, Arf6^{+} but not Rab11^{+} and TrfR^{+} recycling endosomes respond to nerve growth factor (NGF) stimulation, suggesting functional differences in recycling endosome species (Kobayashi and Fukuda, 2013). By immunofluorescent staining of primary hippocampal neurons, we determined the density of Arf6^{+}, Rab11^{+} and Trf^{+} recycling endosomes by software-assisted segmentation (Fig.S5A, B, C) and quantified vesicle-$GABA_AR$ colocalization using object-based colocalization (Fig. S7A, B, C, D; see Methods). We found that the the density of Arf6^{+}, Rab11^{+} and Trf^{+} was each decreased in *Arfgef1*$^{fs/+}$ neuronal cell body (Fig. S6Ai, Bi, Ci), as was the density of these respective vesicles that colocalized with $GABA_AR$ (Fig. 6Ai, Bi, Ci, S7A, B, C). These results suggest either an increase in the dendritic $GABA_AR$ recycling, leading to reduction in retrograde trafficking into the cell body, or increase in the recycling endosome that mature into late endosomes. The former is less likely because our result demonstrated reduction in dendritic surface-bound $GABA_AR$. Findings in dendrites further reinforced this idea: in *Arfgef1*$^{fs/+}$ dendrites, Arf6^{+} recycling endosomes decreased in density compared to wildtype (Fig. S5A, S6Aii), including those that colocalized with $GABA_AR$ (Fig. 6Aii, S7A). In contrast, the density of Rab11^{+} and TrfR^{+} recycling endosomes (Fig. S5B, C, 6Bii, Cii) and those colocalized with $GABA_AR$ (Fig. 6Bii, Cii, S7B, C) in *Arfgef1*$^{fs/+}$ dendrite were comparable to wildtype. These results suggest that *Arfgef1* haploinsufficiency does not only reduced density of Arf6^{+}, Rab11^{+}, TrfR^{+} recycling endosomes in cell body, such haploinsufficiency may also specifically affects Arf6-dependent dendritic $GABA_AR$ recycling.

240 It is useful to consider the impact of *Arfgef1* genotype on the relative ratio of Arf6^{+}, Rab11^{+},
241 and TrfR^{+} recycling endosomes, because of the interelationship between these microorganelles.
242 Pairwise comparisons of mutant to wildtype showed that the recycling endosome ratio was
243 significantly skewed in *Arfgef1*$^{fs/+}$ dendrite (p=0.006) but not in cell body (p=0.252). The
244 imbalance in recycling endosome populations in dendrite could be the reason for the decrease
245 of dendritic surface GABA$_A$R.
246
247 The early endosome is an intermediate organelle, which can either turn into recycling
248 endosomes or mature into lysosomes (Naslavsky and Caplan, 2018). Earlier evidence showed
249 that Arfgef1 also localizes on early endosomes and functions similarly as Arfgef1 localized in
250 the trans-Golgi network (D'Souza et al., 2014). Reduction in the density of early endosomes in
251 dendrite could be the reason for the change in the density of recycling endosomes. However,
252 when compared to wildtype, there were no changes in the density of EEA1^{+} early endosomes
253 in dendrite or cell body of *Arfgef1*$^{fs/+}$ neurons (Fig. S5D, S6Di, ii), as well as the density of
254 early endosomes that colocalized with GABA$_A$R (Fig.6Di, ii, S7D).
255
256 **Accumulation of GABA$_A$R in lysosomes in *Arfgef1*$^{fs/+}$ neurons**
257 The decrease of surface GABA$_A$R accompanied by decrease in recycling endosomes suggest
258 that the internalized receptors might have been targeted elsewhere. It has been shown that
259 internalized GABA$_A$R that fail to recycle back to the plasma membrane are directed to
260 lysosomes for degradation (Kittler et al., 2004). This led us to determine whether reduction in
261 surface GABA$_A$R was accompanied by lysosomal accumulation of GABA$_A$R. Indeed, in cell
262 body and dendrite of *Arfgef1*$^{fs/+}$ neurons, Lamp1^{+} lysosome density (Fig. 6E, Fi,ii), as well as
263 lysosome that colocalized with GABA$_A$R (Fig.6Gi, ii) increased compared to wildtype. This

showed that $GABA_AR$ in *Arfgef1*$^{fs/+}$ neurons were redirected to lysosomes instead of being recycled back plasma membrane.

Discussion

Arfgef1$^{fs/+}$ mice were generated to model a Lennox-Gastaut Syndrome patient heterozygous for a *de novo* mutation that creates a premature translational stop in the Arfgef1 C-terminus, and thus a haploinsufficient state via presumed nonsense-mediated decay. *Arfgef1*$^{fs/+}$ mice do not have spontaneous convulsions, as is sometimes the case with genotypically accurate mouse models of childhood epilepsy that either do not have spontaneous seizures (Frankel et al., 2009; Amendola et al., 2014) or have seizures of a different type than described in the respective patients (Warner et al., 2016; Kovacevic et al., 2018). However, *Arfgef1*$^{fs/+}$ do have a low threshold to induced seizures, indicating clear seizure susceptibility. Their abnormal performance in developmental milestone tasks, modest but significant, also suggests global developmental delay and possibly hypotonia, like the patient. The predicted maturation rate for mouse is 150 times faster than human in the first month. Thus, the age at which the *Arfgef1*$^{fs/+}$ developmental features are most apparent, between ages PND5 and PND7, is equivalent to a 2-3 year child (Flurkey et al., 2007). This very rapid postnatal maturation in mouse may also partly account for compensatory neurodevelopmental features that prevent a more severe outcome, such as spontaneous seizures.

Arfgef1$^{fs/+}$ animals have a normal lifespan, whereas *Arfgef1*$^{fs/fs}$ die perinatally; in agreement with the earlier report of *Arfgef1* knockout mice (Teoh et al., 2017), except the forebrain defect evident at E17.5 in *Arfgef1*$^{fs/fs}$ mice, is more severe. This difference could be due merely to genetic background: the earlier study did not use an inbred strain but rather a mixed 129/SvJ;C57BL/6J background in which hybrid vigor may have mitigated severity.

289

290 The $GABA_AR$ is a membrane-bound ligand-gated ion channel selective for chloride ions
291 (Moroni et al., 2011). Accumulation of $GABA_AR$ at the synaptic site is required for inhibitory
292 synapse formation and for fast synaptic inhibition (Bogdanov et al., 2006). Other than being
293 trafficked from Golgi to plasma membrane (Luscher et al., 2011), surface $GABA_A$ receptors
294 also undergo constitutive endocytosis and then are recycled back to the membrane surface or
295 delivered to lysosome for degradation (Kittler et al., 2000). Our results suggest that both copies
296 of *Arfgef1* are required to maintain normal endosome composition, which is in turn critical for
297 receptor recycling.

298

299 Arl1 recruits Arfgef1 to early endosomes (D'Souza et al., 2014). Internalized membrane surface
300 receptors fed into early endosomes have several fates. Surface receptors stay in early
301 endosomes if they are not quickly recycled to plasma membrane from early endosomes or
302 delivered into recycling endosomes for slow recycling. The early endosomes with surface
303 receptors that are not destinied for recycling then mature into lysosomes for degradation
304 (Kittler et al., 2004; Naslavsky and Caplan, 2018). In *Arfgef1*$^{fs/+}$ neurons, there was no change
305 in dendritic early endosomes density but $Arf6^+$ recycling endosomes were available albeit
306 decreased in density, suggesting that less early endosomes are destinied for recycling – as
307 supported by our observation of decreased $GABA_AR$ on the *Arfgef1*$^{fs/+}$dendrite surface - these
308 vesicles mature into lysosomes, which, in turn, are more abundant in the *Arfgef1*$^{fs/+}$ cell body.

309

310 The imbalance of recycling and early endosome populations may also explain why there are
311 more lysosomes in *Arfgef1*$^{fs/+}$. AP1 and GGAs, recruited by the Arfgef to the trans-Golgi
312 network, are required to regulate lysosomal enzyme trafficking from the trans-Golgi to
313 lysosomes (Le Borgne and Hoflack, 1998; Hirst et al., 2000; Lowery et al., 2013). Depletion

of Arfgef1 alone does not affect the level of GGAs in the trans-Golgi network (Boal and Stephens, 2010; Miyamoto et al., 2018). It has also been demonstrated that the number of synaptic $GABA_AR$s increase in GGA-deficient mouse (Walker et al., 2016). However, depletion of Arfgef1 reduces the formation of AP-1 complex. Notably, such depletion does not entirely eliminate AP-1 (Miyamoto et al., 2018). Since Arfgef2 can compensate for Arfgef1 in the trans-Golgi network (Ramaen et al., 2007), AP-1 and GGAs levels are required for maintaining the network through to lysosomal trafficking, thus the degradation rate would be be maintained in *Arfgef1*$^{fs/+}$ neurons. In our study, although there is significantly less dendritic surface-bound $GABA_AR$, some $GABA_AR$ can still be transported to the membrane surface. Thus, the reduction of surface $GABA_AR$ is most likely due to reduced recycling, leading to increased $GABA_AR$ accumulation in lysosomes.

We can only speculate why *Arfgef1* haploinsufficiency in mouse is less severe than the human disease it models, or why more *ARFGEF1* variants have not been found in epilepsy. Lennox-Gastaut Syndrome is a genetically heterogeneous complex childhood epilepsy, if a primary gene is known at all. *Arfgef1* homozygous knockouts are very severely impaired. One possibility is that a very delicate balance of gene dosage, combined with a limited window of late gestational or early postnatal vulnerability, allows the more rapid mouse postnatal development to push through. A more discrete possibility is that *ARFGEF1* is actually a modifier mutation, requiring another predisposing variant for severe disease. In multiple prior studies, *ARFGEF1* was reported as a candidate together with at least one other gene. For example, in a large Australian family spanning three generations in which *CRH* had been proposed as a EE candidate gene (Wallace et al., 1996), Piro and colleagues later suggested that *ARFGEF1* was also plausible (Piro et al., 2011). In another study of copy number variants (CNV), the authors reported an EE patient with onset of 10 years with *ARFGEF1* and *CSPP1*

as candidate genes (Addis et al., 2018). In our study, the Lennox-Gastaut patient also carried a nonsynonymous *BMP2* variant; while BMP2 is not yet associated with epilepsy at least one study has shown that BMP2 signaling promotes the differentiation of some GABAergic neurons (Yao et al., 2010). Regardless, the specific impact of *Arfgef1* haploinsufficiency on endosomal balance and dendritic vesicle fate is an attractive pathogenic mechanism and therapeutic target opportunity that may apply to other forms of childhood epilepsy.

Materials and Methods

Generation of *Arfgef1* mice

All mice breeding and husbandry were done within the Institute of Comparative Medicine in Columbia University. The mice were kept under a 12-hr day-night cycle with unlimited access to water and food. Mice at two to six-months-old were used for mating. All animal-related procedures were performed according to the guidelines of the Institutional Animal Care and Use Committee (IACUC) of Columbia University. The germline mutation mice were generated in the Genetic Engineering and Technology Core at The Jackson Laboratory (Bar Harbor, ME). In mouse, the *Arfgef1* gene is on Chromosome 1 and consists of 38 exons. Briefly, a guide RNA directing Cas9 endonuclease together with a single-stranded repair template targeting exon 30 was injected into single-cell mouse embryos of C57BL/6NJ line. Founder line were genotyped using PCR (primer F3, 5'-GTCTGAAGTGAAGCACGTTGG-3' and primer R3, 5'-CAGTGGGGTCAACGTGTTATG-3'), restriction enzyme digestion (MwoI; New England Biolabs, R0573L) and DNA sequencing (primer F2, 5'-GTGGCTAGAGAGGCTCGTTTT-3'). Identified founder mice were crossed with wildtype C57BL/6NJ, resulting *Arfgef1*^{fs} line (4-nt deletion in exon 30).

RT-PCR

Total RNA was collected from wildtype and *Arfgef1*$^{fs/+}$ brains at embryonic day 17.5 (E17.5) using TRIzol reagent (Ambion, 15596026). Reverse transcription was performed using SuperScript™ III First-Strand Synthesis SuperMix for qRT-PCR (Invitrogen, 11752-050) according to the manufacturer's protocol. PCR was then performed using primers flanking *Arfgef1* cDNA corresponding to the exons 3-6 (N-terminal DCB domain), exons 13-17 (Sec7 domain), exons 29-31 (mutation site) and exons 31-38 (C-terminal HDS4 domain) with primerd flaking actin as control. The PCR products were subjected to electrophoresis on 2% agarose gels. The primers used in this experiment were listed below.

DCB domain

Forward: 5'- CAC CCT TCC ACC AGT GAA ATC A -3'

Reverse: 5'- TGC TGC CGA TGT CTT TCT CTT TC -3'

Amplicon size: 495bp

Sec7 domain

Forward: 5'- GGA ATT GGC AGC TAC AGT ACA CAG -3'

Reverse: 5'- CCT GTG GAC TGT GAA GGT CTG -3'

Amplicon size: 505bp

Exon 29-31

Forward: 5'- GAC AAC ATG AAA TTG CCA GAA CAG C -3'

Reverse: 5'- GAT ATC CAG GGT GCA GTT ACA CG -3'

Amplicon size: 285bp

HSD4 domain

Forward: 5'- GCT GGA ACT CAT CCA GAC CAT C -3'

Reverse: 5'- TGA GCT TTA AAC CTG CTG TCA CTG -3'

Amplicon size: 524bp

Actin

Forward: 5'- ACG ATA TCG CTG CGC TGG -3'

Reverse: 5'- GAG CAT CGT CGC CCG C -3'

Amplicon size: 72bp

Antibodies

The following primary antibodies were used: Anti-Arfgef1 N-terminal epitope (ThermoFisher Scientific, PA5-54894; Santa Cruz, sc-376790; sc-50391), anti-Arfgef1 C-terminal epitope (Bethyl, A300-998A), Anti-GABA A Receptor with epitope for extracellular domain of the β2,3 subunits (Millipore Sigma, MAB341), anti-synaptophysin (ThermoFisher Scientific, PA1-1043), anti-lamp1 (DSHB, 1D4B), anti-eea1 (R&D Systems, AF8047), anti-transferrin receptor (Abcam, ab84036), anti-Rab11 (ThermoFisher Scientific, 71-5300), anti-Arf6 (ThermoFisher Scientific, PA1-093), anti-map2 (Millipore Sigma, Ab5622), anti-ankG (Santa Cruz, sc-28561), anti-ß-tubulin (Proteintech, 10094-1-AP and 66240-1-Ig), anti-GAPDH (Proteintech, 60004-1-Ig), anti-lamin B1 (Proteintech, 66095-1-lg). The following secondary antibodies were used: Goat anti-mouse HRP-conjugated IgG (Proteintech, SA00001-1), goat anti-rabbit HRP-conjugated IgG (Proteintech, SA00001-2), Goat anti-mouse Alexa Fluor 488-conjugated IgG (ThermoFisher Scientific, A11017), goat anti-rabbit Alexa Fluor 594-conjugated IgG (ThermoFisher Scientific, A11072), goat anti-rat Alexa Fluor 594-conjugated IgG (ThermoFisher Scientific, A11007), donkey anti-sheep NL557-conjugated IgG (R&D Systems, NL010).

414

415 **Western blotting**

416 Brain lysates were collected using the trichloroacetic acid precipitation method. Briefly, the
417 lysates were separated by SDS-PAGE and transferred to Immobilon-PSQ PVDF Membrane
418 (Millipore Sigma, ISEQ00010). The membranes were incubated with primary antibodies
419 overnight at 4°C, followed by incubation with the appropriate HRP-conjugated secondary
420 antibody for 1 hr at room temperature. Samples were washed three times in PBS with 0.05%
421 Tween-20 (PBST) after each step. Signals were developed using Amersham ECL Western
422 Blotting Detection Reagent (GE Healthcare, RPN2106) and visualized using western blot
423 imaging system (Azure Biosystems, Azure C400).

424

425 **Video-EEG**

426 Mice of both sexes, aged 5 weeks and 8 weeks were anesthetized through intraperitoneal
427 injection of 400mg/kg 2,2,2-Tribromoethanol (Sigma Aldrich, T48402). Surgery was
428 performed to drill four burr holes. The first two holes located 1 mm anterior to bregma on both
429 sides. The third hole located 2 mm posterior to bregma on the left side. The fourth hole located
430 over the cerebellum as reference. Four teflon-coated silver wires soldered on a microconnector
431 (Mouser electronics, 575-501101) were placed between dura mater and pia mater and a dental
432 cap was applied. Post-operative mice were given 5mg/kg carprofen (Zoetis, Rimadyl injectable)
433 subcutaneously and a recovery time of 48 hours before electroencephalography (EEG)
434 recording. The recovered mice were then connected to Natus Quantum programmable
435 amplifier (Natus Neurology, 014160) for 24 hours over one day-night cycle. The mice activity
436 was video-recorded simultaneously using a night-vision-enabled Sony IPELA EP500 camera.
437 Differential amplification recordings were recorded pair-wise between the three electrodes and

438 a referential electrode, resulted in a montage of 6 channels for each mouse. The EEG data was
439 analyzed using Natus Database v8.5.1.

440

441 **Seizure susceptibility tests**

442 Electroconvulsive threshold testing was performed in mice 7-10 weeks of age as described
443 previously with minor modification(Frankel et al., 2001)s (Frankel et al., 2001). Briefly, a drop
444 of a topical anesthetic (0.5% tetracaine in 0.9% NaCl) was placed on each eye of a restrained
445 mouse, and current was applied using silver transcorneal electrodes connected to an
446 electroconvulsive stimulator (Ugo Basile model 7801) using the following parameters: 299 Hz
447 frequency 1.6 ms pulse width, 0.2 s pulse duration, variable current. Mice were tested
448 approximately daily in 0.5 mA increments until the minimal clonic forebrain seizure endpoint
449 was reached. For analysis the mean integrated root mean square (iRMS) current is reported for
450 each genotype-sex group.

451 Chemical seizure susceptibility was performed using subcutaneous injection of mice between
452 9 and 10 weeks of age using pentylenetetrazol (PTZ), a GABAA receptor antagonist. Mice
453 were observed for 30 min and incidence of and latency to the first tonic-clonic seizure endpoint
454 was recorded. The PTZ dose of 40 mg/kg was predetermined to be near the threshold for the
455 tonic-clonic seizure endpoint in C57BL/6NJ mice of this age.

456 The Wilcoxon non-parametric rank-sum test with 1000 permutations was used in R to
457 determine permutation *p*-values for elecroconvulsive threshold and for latency to PTZ-induced
458 tonic-clonic seizure.

459

460 **Developmental milestones and ultrasonic vocalization**

461 All pups from the same litter were kept with respective mother throughout the experimental
462 period. They were numbered with tattoo on the soles at PND2 and evaluated for neurological
463 reflexes on PND 3, 5, 7, 9 and 11. Each subject was tested at the same three-hour time window
464 of a day. The pups were weighted each day during the test. For righting reflex test, the pup was
465 placed on its back on a flat and hard surface. The time a pup took to right itself on all four paws
466 was recorded. For negative geotaxis test, the pup was placed with head facing downward on a
467 20 x 20 cm flat wire mesh screen slanted at 45° angle. The time a pup took to turn around and
468 face the angle of 90° and 180° from the starting downward direction was recorded. For vertical
469 screen grasping test, the pups were placed on a 20 x 20 cm flat wire mesh standing vertically
470 at an angle of 90° to a flat surface. The time a pup was able to maintain itself on the mesh wire
471 was recorded. All the times were recorded using a stopwatch for a maximum of 30 seconds (s).
472 All test were carried out under room temperature. The pups were returned to the mother
473 immediately after the tests.

474 Ultrasonic vocalization from a pup being isolated from its mother and littermates was recorded
475 on PND 4, 6, 8 and 10. Briefly, a random pup was removed gently from its nest into an isolation
476 container filled with clean bedding. The container was then placed into a sound attenuating
477 chamber equipped with an UltraSoundGate Condenser Microphone CM 16 (Avisoft
478 Bioacoustics, 40011). The microphone connected to an UltraSoundGate 116 USB audio device
479 (Avisoft Bioacoustics) was linked to a computer installed with Avisoft RECORDER v2.97,
480 where the acoustic data was recorded at a sampling rate of 250,000 Hz in 16 bit format. The
481 software was programmed to filtered away acoustic frequency lower than 15 kHz to reduce
482 background noise interference. Each pup was recorded for 3 min, weighted, and then returned
483 to nest with mother immediately. The number of calls emitted by the pups was counted by an

484 independent operator blinded from the genotypes. The Wilcoxon non-parametric rank-sum test
485 with 1000 permutations was used in R to determine permutation *p*-values.

486

487 **Hematoxylin and eosin staining**

488 Mice of respective ages were perfused. The brains were carefully extracted and cut along the
489 lambda-bregma points. Pieces of brains were fixed in 4% (w/v) paraformaldehyde (PFA) in 0.1
490 M phosphate buffer (PB) at pH 7.4 overnight at 4°C. After serial dehydration steps, the brains
491 were embedded in paraffin (Sigma, P3808). The brains were sectioned at 5 µm thickness using
492 Leica RM2125 microtome. Every tenth section were collected on a glass slide (Matsunami
493 Glass, SUMGP14) and subjected to HE staining. Briefly, the slices were rehydrated and stained
494 with hematoxylin then counterstained with eosin. These slices were subsequently dehydrated
495 using ethanol and xylene and mounted with coverslip using Permount (Fisher Chemical, SP15-
496 500). Histological images were acquired using a Nikon Eclispse E800M light microscope and
497 NIS-elements v4.51. Images were merged using automated function in Photoshop CC 2015.

498

499 ***Ex vivo* single neuron diolistic labeling and spine analysis**

500 The postnatal day (PND) 14 brains were collected and fixed as described above. These brains
501 were transferred into fresh 2% PFA in 0.1 M PB at pH 7.4 and stored at 4°C for up to two
502 months before use. The brains were embedded in 4% agarose and shot with a gene gun (Biorad,
503 1652451) loaded with homemade bullets consisting tungsten microbeads (Biorad, 1652267)
504 coated with DiI (Invitrogen, D282) at 80 PSI. After gentle washing, the brains were immersed
505 in fresh 2% PFA in 0.1 M PB at pH 7.4 and stored in a dark moisten chamber for 3 days at
506 room temperature to allow dye diffusion. Finally, the brains were sliced at 300uM using a
507 vibrotome (Leica, VT1200) and mounted with coverslip using glycerol. Z-stacks images were

acquired immediately using Zeiss LSM-800 confocal microscope and Zen v2.3. The quantification and morphological analysis of spines were done using NeuronStudio v0.9.92. In agreement with literature, the spine shapes were categorized as filopodia, thin, mushroom and stubby (Qiao et al., 2016). Spines with a neck are classified as thin or mushroom based on the head diameter. Spines longer than 3 mm were classified as filopodia. Spines without a neck are classified as stubby.

Primary hippocampal neuron culture

Primary hippocampal neurons were collected according to Fath's method with little modification (Fath et al., 2009). Briefly, hippocampi were dissected from embryonic day (E) 17.5 embryos, dissociated through trituration with the aid of papain (Worthington, LK003178) pre-incubation. A total of 1 x 10^5 cells was plated in 35 mm culture dish containing acid-treated coverslips coated with poly-D-lysine (Sigma-Aldrich, P7886) and laminin (Gibco, 23017015). The primary hippocampal neurons were kept in culture medium containing Neurobasal-A medium (Gibco, 10888022) supplemented with B27 (Gibco, 17504044) and Glutamax (Gibco, 35050061). Cytosine β-D-arabinofuranoside (Sigma-Aldrich, C1768) was added once to a final concentration of 3 µM on the next day after 50% medium change. The cultures were maintained at 37°C with 5% CO_2 in a humidified incubator. Every three days, 50% expensed medium were replaced with fresh culture medium.

Immunofluorescence

DIV14 neurons were fixed for 10 min at 4°C with 4% (w/v) PFA in 0.1 M PB at pH 7.4. The fixed neurons were incubated in blocking buffer containing 5% goat serum (Gibco, 16210064) and 0.1% saponin (Sigma-Aldrich, 47036) in PBS pH 7.4 (Gibco, 10010031) at room temperature for 30 min. Blocked neurons were subsequently incubated with primary antibodies

533 in blocking buffer at 4°C overnight followed by incubation with appropriate secondary
534 antibodies and DAPI in blocking buffer at room temperature for 2 hrs. Samples were washed
535 three times in PBS after each step. The stained neurons on coverslips were mounted on glass
536 slides using Fluoromount-G (Southern Biotech, 0100-01) and sealed with nail polish after
537 drying at room temperature overnight. Z-stacks images were acquired using Zeiss LSM-800
538 confocal microscope and Zen v2.3. The quantification and analysis of labeled vesicle and
539 GABA$_A$R puncta were done using Imaris v9.2.1 software. Due to the limitation of the point
540 spread function (PSF) for tiny objects in confocal microscopy, colocalization is quantified
541 using an object-based method (Dunn et al., 2011). Briefly, vesicle and GABA$_A$R puncta stained
542 with antibodies in cell body or dendrite are recognized and segmented in different channels
543 using Imaris v9.2.1. One GABA$_A$R colocalized with one vesicle is defined as one GABA$_A$R
544 punctum localizes within 1 μm proximity of one vesicle punctum, center to center. There were
545 no significant differences found in the dendrite length and the cell body area where the data
546 were collected. Therefore, the number of puncta in dendrite was normalized using dendrite
547 length (μm) and the number of puncta in cell body was normalized using cell body area (μm^2).
548 The normalized numbers were presented as density (in dendrite, vesicle number per μm; in cell
549 body, vesicle number per μm^2).
550
551 For statistical analysis of puncta counts, a log-Poisson mixed model was run using the lme4
552 package in R (www.R-project.org), with cell body area or dendrite length as a respective
553 covariate and a random effects term included to correct for significant overdispersion in the
554 count data. To determine whether endosome ratios differed between mutant genotype and
555 wildtype, genotype x vesicle type interaction terms were included in a similar model which
556 also included a fixed term for the individual biological from which ratios examined. Statistical
557 comparisons in this study were considered significant if the p-value is less than 0.05.

558

559 **Single cell patch-clamp recordings**

560 To assess synaptic activity, electrophysiological recordings were carried out from dissociated
561 hippocampal neurons plated at a density of 50000 cells on 15 mm diameter glass coverslips
562 and cultured for 13-15 days. Recordings were made in voltage clamp whole-cell configuration
563 using a Multiclamp 700B amplifier and a Digidata 1550 digital-to-analogue converter (both
564 from Molecular Devices) at a 10 kHz sample frequency. Patch pipettes were fabricated with a
565 P-97 pipette puller (Sutter Instruments) using 1.5 mm outer diameter, 1.28 mm inner diameter
566 filamented capillary glass (World Precision Instruments). The external recording solution
567 contained (in mM): NaCl 145, KCl 5, HEPES 10, Glucose 10, $CaCl_2$ 2, $MgCl_2$ 2, 0.001
568 tetrodotoxin, pH 7.3 with NaOH, and osmolality adjusted to 325 mOsm using sucrose. A
569 cesium-based pipette solution contained (in mM): cesium methanesulfonate 130, sodium
570 methanesulfonate 10, EGTA 10, $CaCl_2$ 1, HEPES 10, TEA-Cl 10, MgATP 5, Na_2GTP 0.5,
571 QX-314 5, pH 7.2 with CsOH, adjusted to 290 mOsm with sucrose. Pipettes had final resistance
572 of approximately 5 MΩ when filled with internal solution. Uncompensated series resistance
573 was <15 MΩ. Series resistance and membrane capacitance were electrically compensated to
574 approximately 70%. Miniature excitatory postsynaptic currents (mEPSCs) and miniature
575 inhibitory postsynaptic currents (mIPSCs), were recorded from the same cell by holding the
576 cells at -60 and 0 mV, respectively. Recordings were acquired for a period of 5 minutes. All
577 recordings were carried out at room temperature (21 – 23 °C). Miniature events were detected
578 offline with Clampfit 12.7 (Molecular Devices) using the template matching function and a
579 minimum threshold of 5 pA. Each event was manually inspected to determine inclusion or
580 rejection in analysis. Further analysis was carried out using R (www.R-project.org).

581

582 **References**

583 Addis L, Sproviero W, Thomas SV, Caraballo RH, Newhouse SJ, Gomez K, Hughes E, Kinali
584 M, McCormick D, Hannan S, Cossu S, Taylor J, Akman CI, Wolf SM, Mandelbaum
585 DE, Gupta R, van der Spek RA, Pruna D, Pal DK (2018) Identification of new risk
586 factors for rolandic epilepsy: CNV at Xp22.31 and alterations at cholinergic synapses.
587 J Med Genet 55:607-616.
588 Amendola E, Zhan Y, Mattucci C, Castroflorio E, Calcagno E, Fuchs C, Lonetti G, Silingardi
589 D, Vyssotski AL, Farley D, Ciani E, Pizzorusso T, Giustetto M, Gross CT (2014)
590 Mapping pathological phenotypes in a mouse model of CDKL5 disorder. PLoS One
591 9:e91613.
592 Boal F, Stephens DJ (2010) Specific functions of BIG1 and BIG2 in endomembrane
593 organization. PLoS One 5:e9898.
594 Bogdanov Y, Michels G, Armstrong-Gold C, Haydon PG, Lindstrom J, Pangalos M, Moss SJ
595 (2006) Synaptic GABAA receptors are directly recruited from their extrasynaptic
596 counterparts. EMBO J 25:4381-4389.
597 D'Souza RS, Semus R, Billings EA, Meyer CB, Conger K, Casanova JE (2014) Rab4
598 orchestrates a small GTPase cascade for recruitment of adaptor proteins to early
599 endosomes. Curr Biol 24:1187-1198.
600 Dunn KW, Kamocka MM, McDonald JH (2011) A practical guide to evaluating colocalization
601 in biological microscopy. Am J Physiol Cell Physiol 300:C723-742.
602 Epi4K Consortium et al. (2013) De novo mutations in epileptic encephalopathies. Nature
603 501:217-221.
604 Fath T, Ke YD, Gunning P, Gotz J, Ittner LM (2009) Primary support cultures of hippocampal
605 and substantia nigra neurons. Nat Protoc 4:78-85.
606 Ferhat AT, Torquet N, Le Sourd AM, de Chaumont F, Olivo-Marin JC, Faure P, Bourgeron T,
607 Ey E (2016) Recording Mouse Ultrasonic Vocalizations to Evaluate Social
608 Communication. J Vis Exp.
609 Flurkey K, Currer JM, Harrison DE (2007) The Mouse in Aging Research.
610 Frankel WN, Taylor L, Beyer B, Tempel BL, White HS (2001) Electroconvulsive thresholds
611 of inbred mouse strains. Genomics 74:306-312.
612 Frankel WN, Yang Y, Mahaffey CL, Beyer BJ, O'Brien TP (2009) Szt2, a novel gene for
613 seizure threshold in mice. Genes Brain Behav 8:568-576.
614 Galindo A, Soler N, McLaughlin SH, Yu M, Williams RL, Munro S (2016) Structural Insights
615 into Arl1-Mediated Targeting of the Arf-GEF BIG1 to the trans-Golgi. Cell Rep
616 16:839-850.
617 Hill JM, Lim MA, Stone MM (2008) Developmental Milestones in the Newborn Mouse. In:
618 Neuropeptide Techniques (I. G, ed), pp 131-149: Humana Press.
619 Hirst J, Lui WW, Bright NA, Totty N, Seaman MN, Robinson MS (2000) A family of proteins
620 with gamma-adaptin and VHS domains that facilitate trafficking between the trans-
621 Golgi network and the vacuole/lysosome. J Cell Biol 149:67-80.
622 Jain P, Sharma S, Tripathi M (2013) Diagnosis and management of epileptic encephalopathies
623 in children. Epilepsy Res Treat 2013:501981.
624 Kittler JT, Delmas P, Jovanovic JN, Brown DA, Smart TG, Moss SJ (2000) Constitutive
625 endocytosis of GABAA receptors by an association with the adaptin AP2 complex
626 modulates inhibitory synaptic currents in hippocampal neurons. J Neurosci 20:7972-
627 7977.
628 Kittler JT, Thomas P, Tretter V, Bogdanov YD, Haucke V, Smart TG, Moss SJ (2004)
629 Huntingtin-associated protein 1 regulates inhibitory synaptic transmission by
630 modulating gamma-aminobutyric acid type A receptor membrane trafficking. Proc Natl
631 Acad Sci U S A 101:12736-12741.

632 Kobayashi H, Fukuda M (2013) Arf6, Rab11 and transferrin receptor define distinct
633 populations of recycling endosomes. Commun Integr Biol 6:e25036.
634 Kovacevic J, Maroteaux G, Schut D, Loos M, Dubey M, Pitsch J, Remmelink E, Koopmans B,
635 Crowley J, Cornelisse LN, Sullivan PF, Schoch S, Toonen RF, Stiedl O, Verhage M
636 (2018) Protein instability, haploinsufficiency, and cortical hyper-excitability underlie
637 STXBP1 encephalopathy. Brain 141:1350-1374.
638 Le Borgne R, Hoflack B (1998) Mechanisms of protein sorting and coat assembly: insights
639 from the clathrin-coated vesicle pathway. Curr Opin Cell Biol 10:499-503.
640 Le K, Li CC, Ye G, Moss J, Vaughan M (2013) Arf guanine nucleotide-exchange factors BIG1
641 and BIG2 regulate nonmuscle myosin IIA activity by anchoring myosin phosphatase
642 complex. Proc Natl Acad Sci U S A 110:E3162-3170.
643 Li C, Chen S, Yu Y, Zhou C, Wang Y, Le K, Li D, Shao W, Lu L, You Y, Peng J, Huang H,
644 Liu P, Shen X (2014) BIG1, a brefeldin A-inhibited guanine nucleotide-exchange factor,
645 is required for GABA-gated Cl(-) influx through regulation of GABAA receptor
646 trafficking. Mol Neurobiol 49:808-819.
647 Lin S, Zhou C, Neufeld E, Wang YH, Xu SW, Lu L, Wang Y, Liu ZP, Li D, Li C, Chen S, Le
648 K, Huang H, Liu P, Moss J, Vaughan M, Shen X (2013) BIG1, a brefeldin A-inhibited
649 guanine nucleotide-exchange protein modulates ATP-binding cassette transporter A-1
650 trafficking and function. Arterioscler Thromb Vasc Biol 33:e31-38.
651 Lowery J, Szul T, Styers M, Holloway Z, Oorschot V, Klumperman J, Sztul E (2013) The Sec7
652 guanine nucleotide exchange factor GBF1 regulates membrane recruitment of BIG1
653 and BIG2 guanine nucleotide exchange factors to the trans-Golgi network (TGN). J
654 Biol Chem 288:11532-11545.
655 Luscher B, Fuchs T, Kilpatrick CL (2011) GABAA receptor trafficking-mediated plasticity of
656 inhibitory synapses. Neuron 70:385-409.
657 Manolea F, Claude A, Chun J, Rosas J, Melancon P (2008) Distinct functions for Arf guanine
658 nucleotide exchange factors at the Golgi complex: GBF1 and BIGs are required for
659 assembly and maintenance of the Golgi stack and trans-Golgi network, respectively.
660 Mol Biol Cell 19:523-535.
661 Miyamoto Y, Torii T, Tago K, Tanoue A, Takashima S, Yamauchi J (2018) BIG1/Arfgef1 and
662 Arf1 regulate the initiation of myelination by Schwann cells in mice. Sci Adv
663 4:eaar4471.
664 Moroni M, Biro I, Giugliano M, Vijayan R, Biggin PC, Beato M, Sivilotti LG (2011) Chloride
665 ions in the pore of glycine and GABA channels shape the time course and voltage
666 dependence of agonist currents. J Neurosci 31:14095-14106.
667 Nakai W, Kondo Y, Saitoh A, Naito T, Nakayama K, Shin HW (2013) ARF1 and ARF4
668 regulate recycling endosomal morphology and retrograde transport from endosomes to
669 the Golgi apparatus. Mol Biol Cell 24:2570-2581.
670 Naslavsky N, Caplan S (2018) The enigmatic endosome - sorting the ins and outs of endocytic
671 trafficking. J Cell Sci 131.
672 Piro RM, Molineris I, Ala U, Di Cunto F (2011) Evaluation of candidate genes from orphan
673 FEB and GEFS+ loci by analysis of human brain gene expression atlases. PLoS One
674 6:e23149.
675 Qiao H, Li MX, Xu C, Chen HB, An SC, Ma XM (2016) Dendritic Spines in Depression: What
676 We Learned from Animal Models. Neural Plast 2016:8056370.
677 Ramaen O, Joubert A, Simister P, Belgareh-Touze N, Olivares-Sanchez MC, Zeeh JC,
678 Chantalat S, Golinelli-Cohen MP, Jackson CL, Biou V, Cherfils J (2007) Interactions
679 between conserved domains within homodimers in the BIG1, BIG2, and GBF1 Arf
680 guanine nucleotide exchange factors. J Biol Chem 282:28834-28842.

Ren Y, Suter DM (2016) Increase in Growth Cone Size Correlates with Decrease in Neurite Growth Rate. Neural Plast 2016:3497901.

Saeki N, Tokuo H, Ikebe M (2005) BIG1 is a binding partner of myosin IXb and regulates its Rho-GTPase activating protein activity. J Biol Chem 280:10128-10134.

Shen X, Xu KF, Fan Q, Pacheco-Rodriguez G, Moss J, Vaughan M (2006) Association of brefeldin A-inhibited guanine nucleotide-exchange protein 2 (BIG2) with recycling endosomes during transferrin uptake. Proc Natl Acad Sci U S A 103:2635-2640.

Shen X, Meza-Carmen V, Puxeddu E, Wang G, Moss J, Vaughan M (2008) Interaction of brefeldin A-inhibited guanine nucleotide-exchange protein (BIG) 1 and kinesin motor protein KIF21A. Proc Natl Acad Sci U S A 105:18788-18793.

Teoh JJ, Iwano T, Kunii M, Atik N, Avriyanti E, Yoshimura SI, Moriwaki K, Harada A (2017) BIG1 is required for the survival of deep layer neurons, neuronal polarity, and the formation of axonal tracts between the thalamus and neocortex in developing brain. PLoS One 12:e0175888.

Trachtenberg JT, Chen BE, Knott GW, Feng G, Sanes JR, Welker E, Svoboda K (2002) Long-term in vivo imaging of experience-dependent synaptic plasticity in adult cortex. Nature 420:788-794.

Walker KR, Modgil A, Albrecht D, Lomoio S, Haydon PG, Moss SJ, Tesco G (2016) Genetic Deletion of the Clathrin Adaptor GGA3 Reduces Anxiety and Alters GABAergic Transmission. PLoS One 11:e0155799.

Wallace RH, Berkovic SF, Howell RA, Sutherland GR, Mulley JC (1996) Suggestion of a major gene for familial febrile convulsions mapping to 8q13-21. J Med Genet 33:308-312.

Warner TA, Shen W, Huang X, Liu Z, Macdonald RL, Kang JQ (2016) Differential molecular and behavioural alterations in mouse models of GABRG2 haploinsufficiency versus dominant negative mutations associated with human epilepsy. Hum Mol Genet 25:3192-3207.

Wright J, Kahn RA, Sztul E (2014) Regulating the large Sec7 ARF guanine nucleotide exchange factors: the when, where and how of activation. Cell Mol Life Sci 71:3419-3438.

Yamaji R, Adamik R, Takeda K, Togawa A, Pacheco-Rodriguez G, Ferrans VJ, Moss J, Vaughan M (2000) Identification and localization of two brefeldin A-inhibited guanine nucleotide-exchange proteins for ADP-ribosylation factors in a macromolecular complex. Proc Natl Acad Sci U S A 97:2567-2572.

Yao M, Niu G, Sheng Z, Wang Z, Fei J (2010) Identification of a Smad4/YY1-recognized and BMP2-responsive transcriptional regulatory module in the promoter of mouse GABA transporter subtype I (Gat1) gene. J Neurosci 30:4062-4071.

Zhao X, Lasell TK, Melancon P (2002) Localization of large ADP-ribosylation factor-guanine nucleotide exchange factors to different Golgi compartments: evidence for distinct functions in protein traffic. Mol Biol Cell 13:119-133.

Zhou C, Li C, Li D, Wang Y, Shao W, You Y, Peng J, Zhang X, Lu L, Shen X (2013) BIG1, a brefeldin A-inhibited guanine nucleotide-exchange protein regulates neurite development via PI3K-AKT and ERK signaling pathways. Neuroscience 254:361-368.

Figure 1

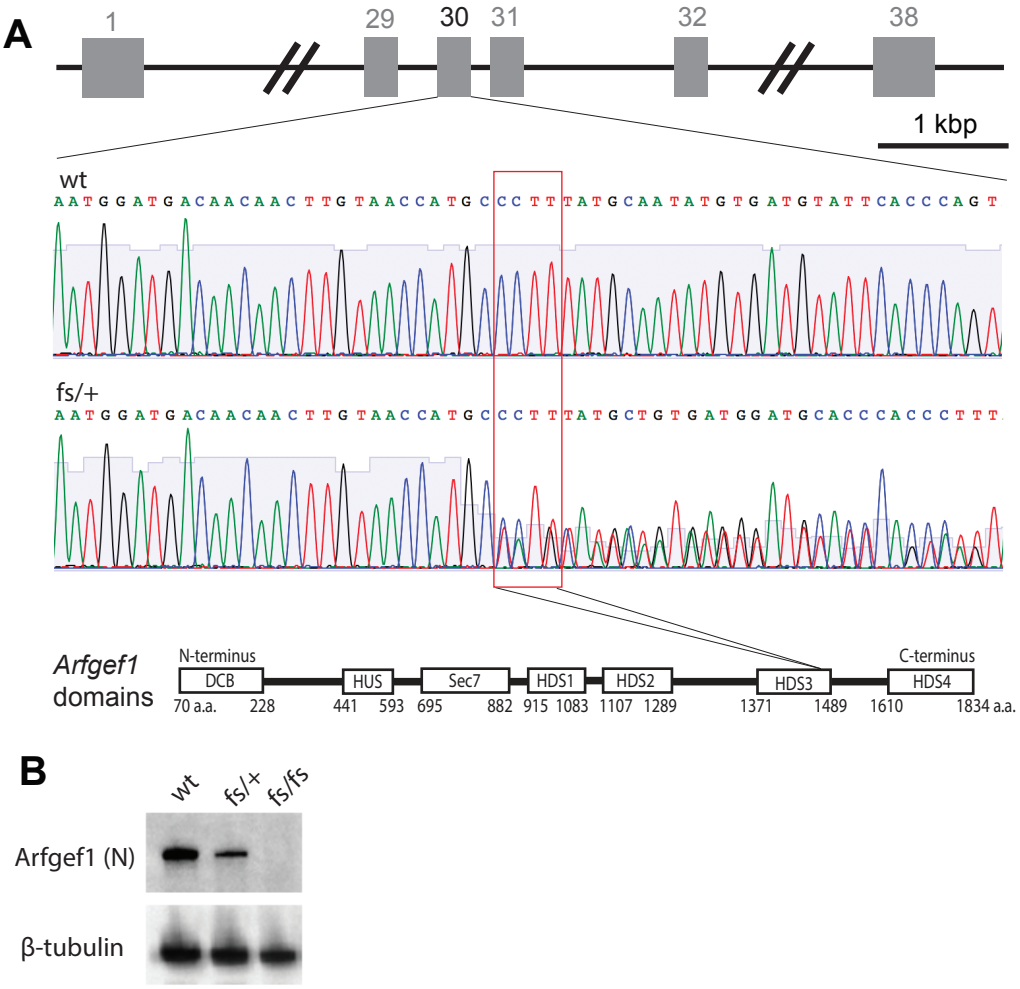

Figure 1. *Generation and genotyping of Arfgef1*^{fs} *mice.* ***A***, The CRISPR/Cas9 targeting *Arfgef1* exon 30 on mouse Chromosome 1 resulted in a 4-nt frameshift mutation (*Arfgef1*^{fs}). The heterozygotes (*Arfgef1*$^{fs/+}$) were verified with Sanger sequencing. The red box shows the sites of mutation for *Arfgef1*^{fs} correspond to HDS3 domain in Arfgef1 protein. ***B***, The western blot was performed using E17.5 brain lysate (n=3 animals per genotype) and detected using antibody targeting Arfgef1 based on an N-terminal epitope, using ß-tubulin as loading control.

Figure 2

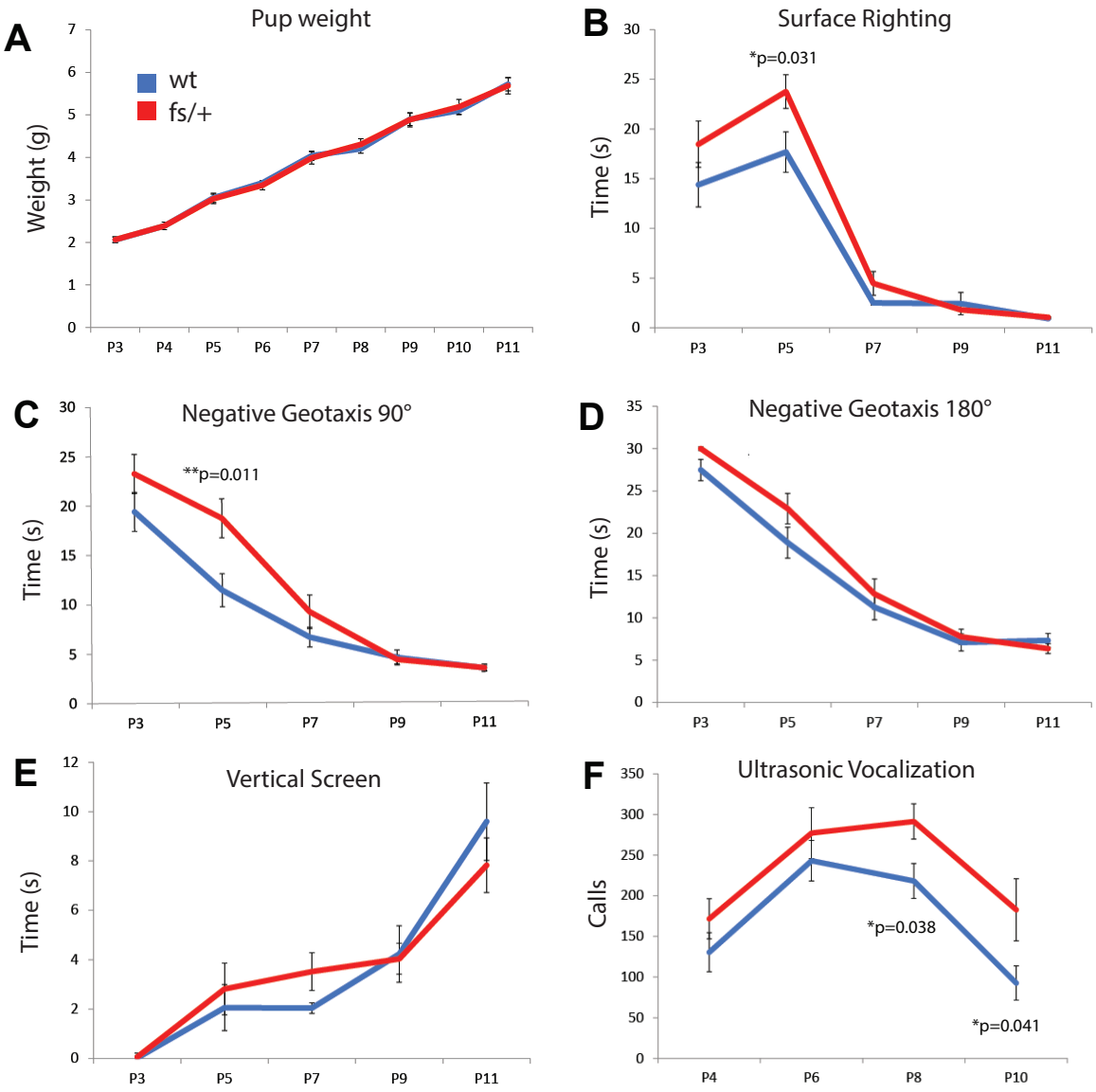

Figure 2. *Developmental milestone and ultrasonic vocalization of Arfgef1*$^{fs/+}$ *pups.* ***A***, The weight of *Arfgef1*$^{fs/+}$ and wildtype pups from PND3 to PND11 is statistically similar. ***B***, ***C***, The time required for surface righting, negative geotaxis 90° of *Arfgef1*$^{fs/+}$ pups is statistically slower than wildtype at PND5. ***D***, ***E***, There is no difference observed in the time for *Arfgef1*$^{fs/+}$ and wildtype pups to accomplish negative geotaxis 180° task or to hold on a vertical screen. ***F***, The ultrasonic calls are statistically higher at PND8 and PND10 for *Arfgef1*$^{fs/+}$ pups compared to wildtype pups. Data are collected from pups of both sexes. wildtype, n=22 animals; *Arfgef1*$^{fs/+}$, n=23 animals from 7 litters. Permutation p-values shown were determined using the Wilcoxon rank-sum test.

Figure 3

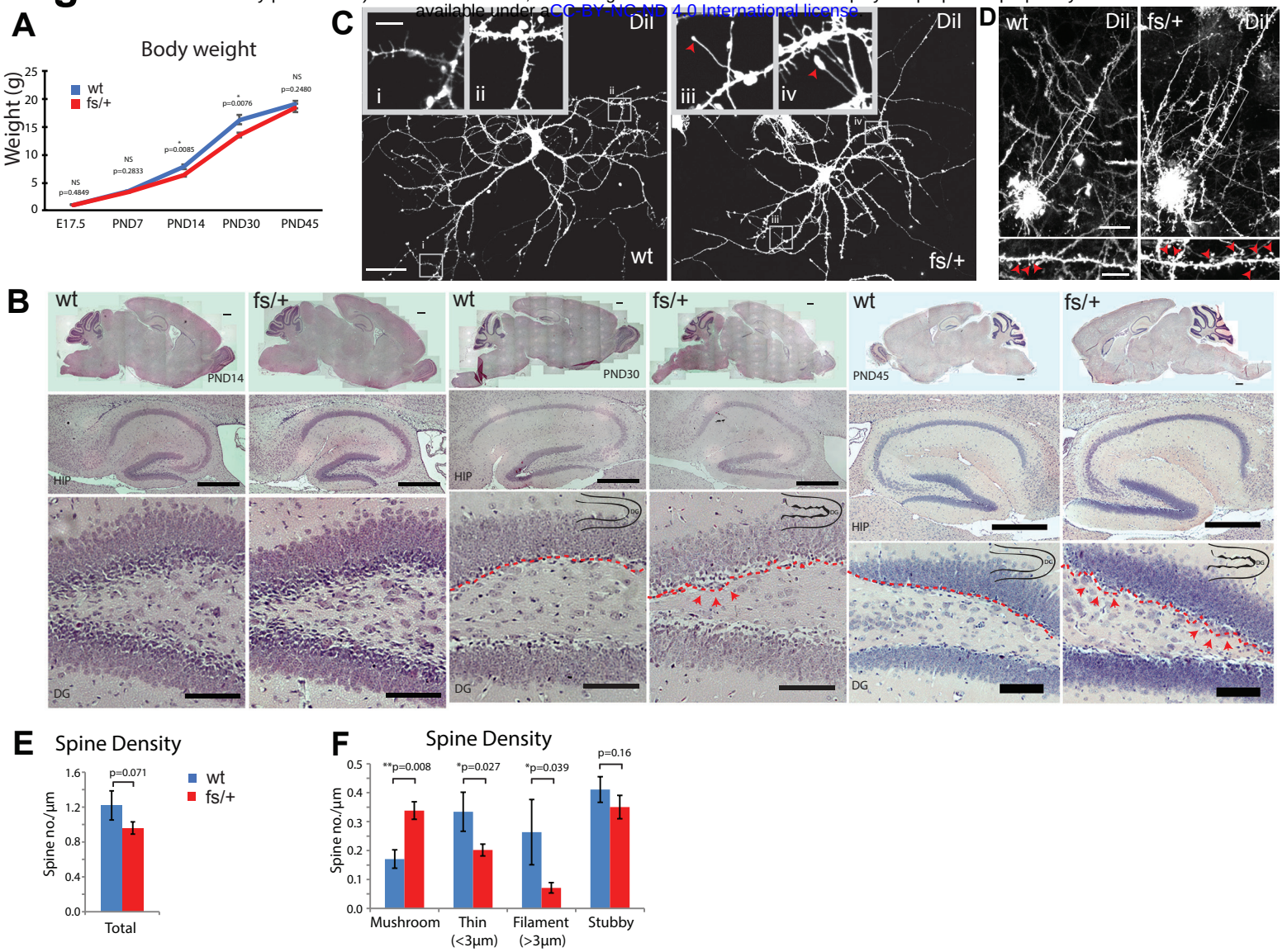

Figure 3. *Morphological characterization of Arfgef1*$^{fs/+}$ *mice.* ***A***, The body weight of *Arfgef1*$^{fs/+}$ mice is statistically lower at PND14 and PND30 compared to wildtype mice. E17.5, wildtype, n=16; *Arfgef1*$^{fs/+}$, n=12 from 4 litters; PND14, 30 and 45, wildtype, n=7 mice; *Arfgef1*$^{fs/+}$, n=8 mice from 5 litters. ***B***, The HE-stained sagittal sections shows irregular bumps (red arrowheads) along *Arfgef1*$^{fs/+}$ dentate gyrus lining (red dotted lines) at PND30 and PND45. n=3 animals per genotype for each time-point. Scale bars, sagittal sections, 500 µm; HIP, 500 µm; DG, 100 µm. ***C***, In DIV14 culture, there are filamentous tertiary structures with large growth cones (red arrowheads) appeared on *Arfgef1*$^{fs/+}$ neurons. wildtype, 4 neurons from 1 animals; *Arfgef1*$^{fs/+}$, n=11 neurons from 3 animals. Scale bars, 50 µm; inset, 10 µm. ***D***, Single deep layer neuron is labeled using diolistic method in PND14 deep layer neurons. Mushroom spines were marked by red arrowheads. ***E*** & ***F***, The total spine density is similar between *Arfgef1*$^{fs/+}$ neurons and wildtype neurons. However, spine subtype density (mushroom, thin and filament) are significantly different. Wildtype and *Arfgef1*$^{fs/+}$, n=3 animals each. Scale bars, 20 µm; enlarged box, 10 µm. Data are collected from mice of both sexes. HIP, hippocampus; DG, dentate gyrus.

Figure 4

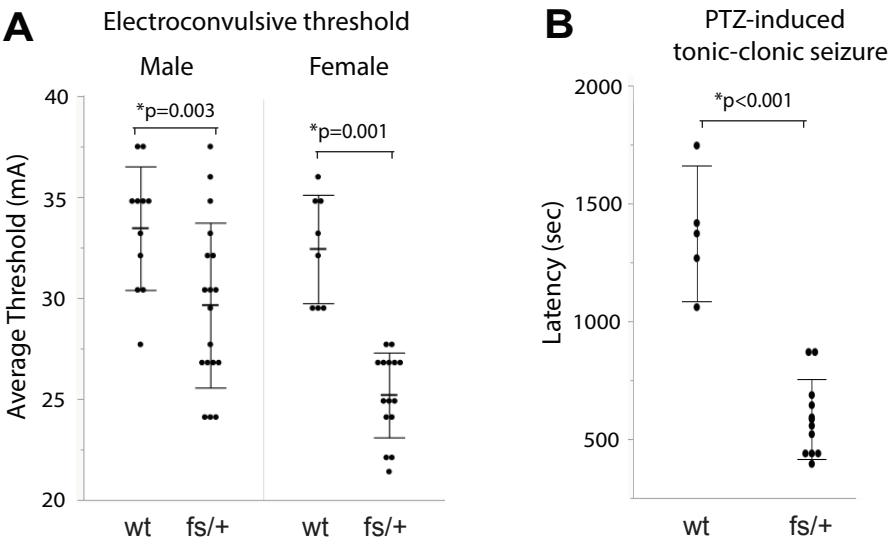

Figure 4. *Seizure susceptibility of Arfgef1*$^{fs/+}$ *mice.* ***A***, Electroconvulsive threshold to the minimal clonic seizure endpoint is significantly lower in *Arfgef1*$^{fs/+}$ mice of both sexes (male, wildtype, n=11; *Arfgef1*$^{fs/+}$, n= 18; female, wildtype, n=11; *Arfgef1*$^{fs/+}$, n= 15). ***B***, The latency for PTZ-induced seizure is significantly lower for *Arfgef1*$^{fs/+}$ mice at 9- to 10-week old. wildtype, n=4; *Arfgef1*$^{fs/+}$, n= 11. Permutation p-values shown were determined using the Wilcoxon rank-sum test.

Figure 5

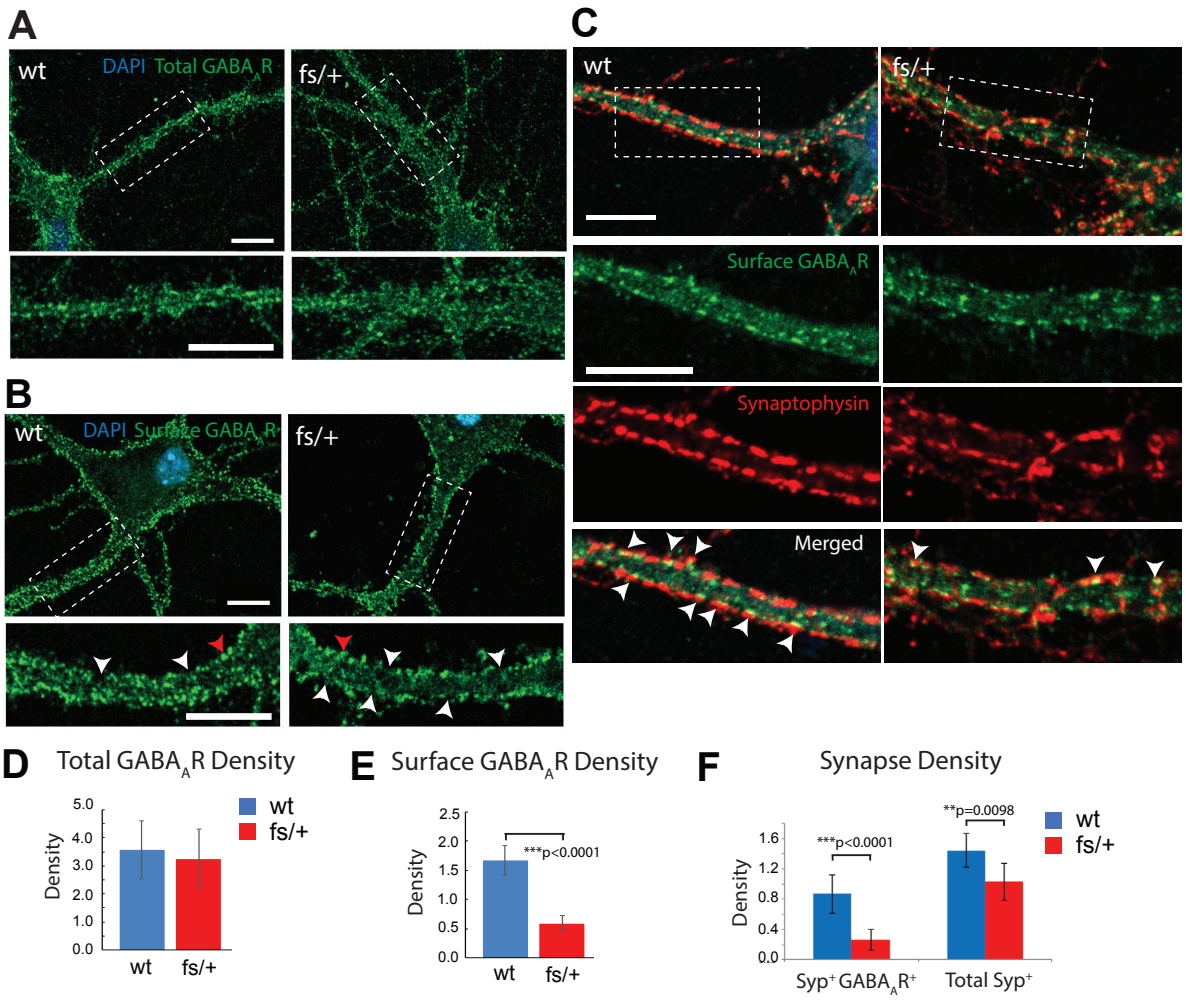

Figure 5. *Membrane surface GABA$_A$R and synaptic GABA$_A$R distribution in Arfgef1$^{fs/+}$ neurons.* ***A***, There is no difference in the localization of total GABA$_A$R puncta in proximal dendrite. ***B***, GABA$_A$R localize on dendritic surface (representative punctum pointed by red arrowheads) at DIV14. The region without GABA$_A$R puncta on dendritic surface are marked by white arrowheads Surface GABA$_A$R, wildtype, n=19:4 (# neurons:# mice); *Arfgef1*$^{fs/+}$, n=23:7. Total GABA$_A$R, wildtype, n=19:4; *Arfgef1*$^{fs/+}$, n=23:7. All scale bars, 10 µm. ***C***, At DIV14, the synaptic GABA$_A$R puncta (white arrowheads) on dendritic surface reduced on *Arfgef1*$^{fs/+}$ dendrite. wildtype, n=19:4; *Arfgef1*$^{fs/+}$, n=12:4. All scale bars, 10 µm. ***D***, ***E***, Graphs show quantification of the dendritic surface GABA$_A$R density and total GABA$_A$R density in dendrite. ***F***, Graph shows the synaptic GABA$_A$R density and total synapse density on dendritic surface. Density is defined as punctum number per dendritic length in µm.

Figure 6

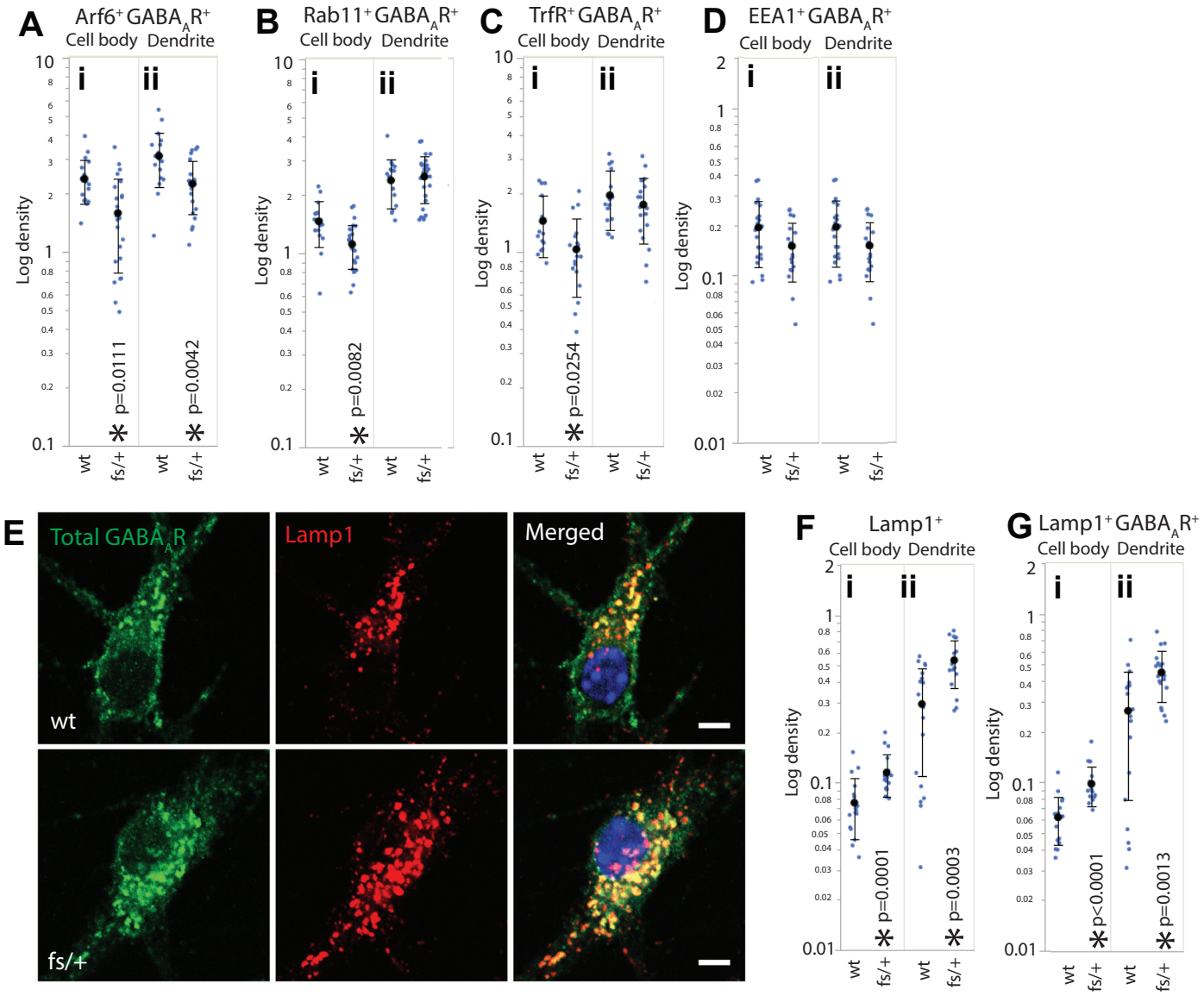

Figure 6. *Distribution of intracellular vesicles colocalized with GABA$_A$R in wildtype and Arfgef1$^{fs/+}$ DIV14 neurons.* ***A***, ***B***, ***C***, ***D***, Graphs show the density of GABA$_A$R colocalized with Arf6$^+$, Rab11$^+$, TrfR$^+$ recycling endosomes and EEA1$^+$ early endosomes in cell body and dendrite. Densities are displayed in log scale. Density in cell body and dendrite is defined as colocalized punctum number per cell body area (μm^2) and the punctum number per dendritic length (μm) respectively. Arf6$^+$, wildtype, n=19:4 (# neurons:# mice); *Arfgef1*$^{fs/+}$, n=23:7. Rab11$^+$, wildtype, n=16:4; *Arfgef1*$^{fs/+}$, n=27:7; TrfR$^+$, wildtype, n=15 :4; *Arfgef1*$^{fs/+}$, n=18:3; EEA1$^+$, wildtype, n=21:6; *Arfgef1*$^{fs/+}$, n=19:5. ***E***, The number of Lamp$^+$ lysosomes and GABA$_A$R-containing lysosomes increase in *Arfgef1*$^{fs/+}$ neurons. ***F*** & ***G***, Graphs show the density of Lamp1$^+$ lysosome and Lamp1$^+$GABA$_A$R$^+$ lysosomes in the cell body or dendrite. wildtype, n=18:6; *Arfgef1*$^{fs/+}$, n=18:5. All scale bars, 5 μm. Density is shown in log scale. Vesicle densities in cell body and dendrite are defined as punctum number per cell body area (μm^2) and the punctum number per dendritic length (μm) respectively.